Materials Science & Engineering A 690 (2017) 1–5

Contents lists available at ScienceDirect

Materials Science & Engineering A

journal homepage: www.elsevier.com/locate/msea

Short communication

Effect of thermal cycling on martensitic transformation and mechanical strengthening of stainless steels – A phase-field study

Hemantha Kumar Yeddu[a,*], Brian A. Shaw[a], Marcel A.J. Somers[b]

[a] School of Mechanical and Systems Engineering, Newcastle University, Newcastle upon Tyne NE1 7RU, United Kingdom
[b] Department of Mechanical Engineering, Technical University of Denmark (DTU), 2800 Kgs. Lyngby, Denmark

ARTICLE INFO

Keywords:
Phase-field model
Martensitic transformation
Reversion
Microstructure
Thermal cycling
Steels

ABSTRACT

A 3D elastoplastic phase-field model is used to study the effect of thermal cycling on martensitic transformation as well as on mechanical strengthening of both austenite and martensite in stainless steel. The results show that with an increasing number of thermal cycles, martensite becomes more stable. Increase in strain, plastic strain and strain hardening lead to strengthening of austenite.

1. Introduction

Phase transformations play an important role in enhancing the mechanical properties of stainless steels. The solid state phase transformation of austenite to martensite, known as martensitic transformation, occurs during quenching and imparts significant strength to steels. Reverse phase transformation of martensite to austenite occurs during intercritical annealing and has been reported to improve the yield strength, by grain refinement, and the ductility of steels [1–3].

Reversion of martensite can occur either by a shear mechanism or a diffusion-controlled mechanism. During reversion by a shear mechanism, dislocations from martensite are inherited into reversed austenite and thereby increase the ductility of steels [1,4]. Morevoer, reversion of martensite leads to grain refinement [1,2,5,6] and grain boundary strengthening [7], which are reported to be effective strengthening mechanisms. Grain refinement can lead to reduction of M_s temperature [8], increased retained austenite [9,10] and dislocation density [11].

Owing to the importance of martensite formation, reverse phase transformation and grain refinement in enhancing the mechanical properties of steels, several thermo-mechanical processing methods have been developed [1,6,12]. Thermal cycling, i.e. repeated quenching and subsequent heating, has proved to be an effective way of grain refinement and strengthening of steels [10]. Durlu reported an increase in dislocation density and strength after thermal cycling of Fe-Ni-C single cystals [13]. Alaei et al. have recently showed that dislocations are inherited from martensite to reversed austenite and that the dislocation density as well as the yield strength increase with increasing number of thermal cycles in an Fe-Ni-C TRIP steel [14]. Although the experimental studies showed that thermal cycling leads to strengthening of steels [10,13,14], it is essential to study the role of austenite and martensite in mechanical strengthening due to thermal cycling.

Several constitutive and phenomenological models have been proposed to study martensite formation and the relation between phase transformation and plasticity [15–17]. The phase-field approach [18,19] has been successfully applied to study martensitic transformation and other solid state phase transformations [20–28] as well as the reversion of martensite to austenite by a shear mechanism [27,29–31]. In the present work, the effect of thermal cycling on martensite formation and reversion of martensite by a shear mechanism as well as on mechanical strengthening of stainless steel is studied, by using a 3D elastoplastic phase-field model [20,29].

2. Phase-field model

The phase-field equation governing the microstructure evolution is given by:

$$\frac{\partial \eta_p}{\partial t} = -\sum_{q=1}^{q=v} L_{pq}\frac{\delta G}{\delta \eta_q} \tag{1}$$

where η_q is the phase field variable that tracks the evolution of martensite, v is the total number of martensite variants and L_{pq} is a matrix of kinetic parameters. Martensite variants (laths), which form in 24 different crystallographic orientations according to the Kurdjumov-

* Corresponding author.
E-mail addresses: hemanth.yeddu@ncl.ac.uk, hemu23@gmail.com (H.K. Yeddu).

http://dx.doi.org/10.1016/j.msea.2017.02.085
Received 23 September 2016; Received in revised form 21 February 2017; Accepted 22 February 2017
Available online 24 February 2017

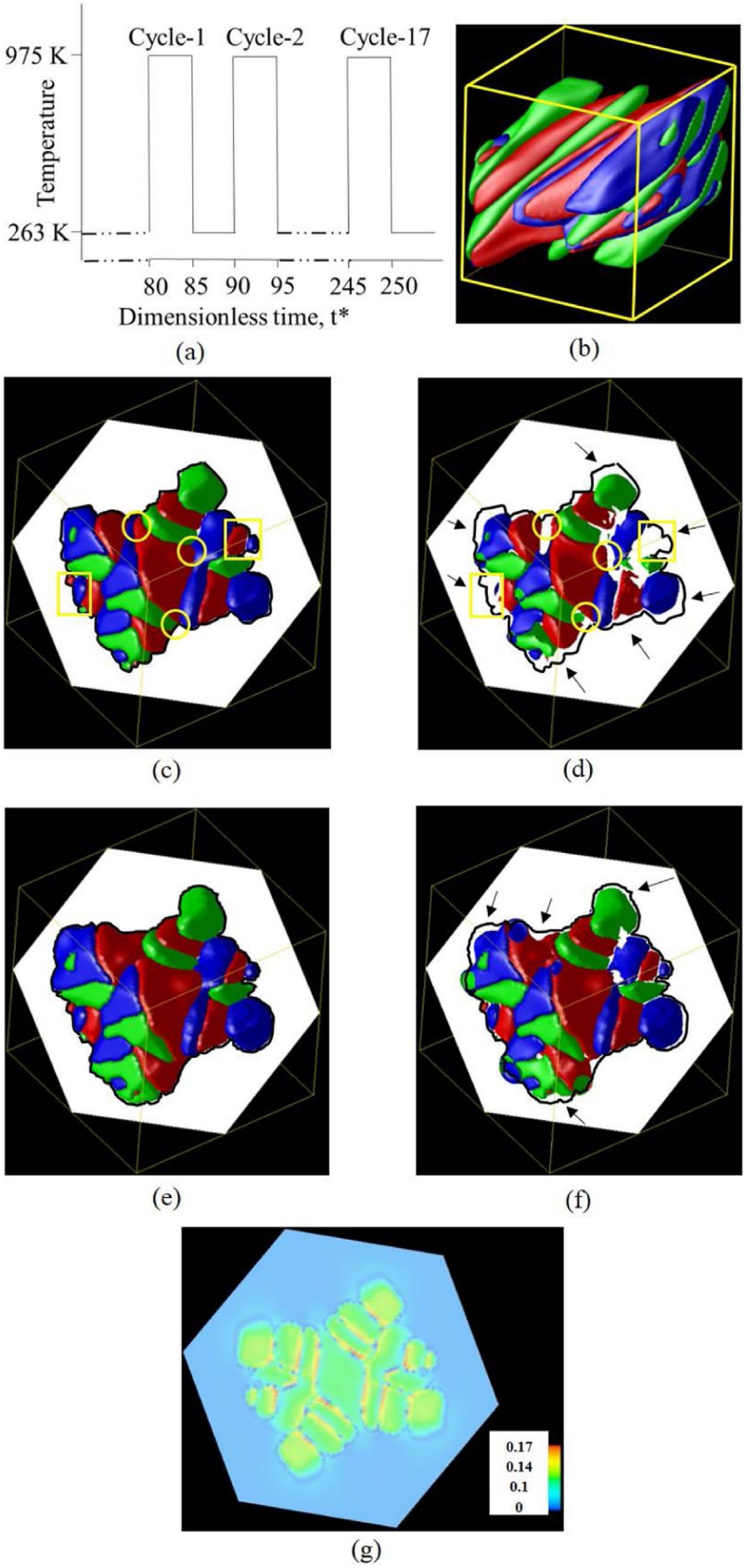

Fig. 1. (a) Schematic of the simulated thermal cycling process. Microstructures at (b) t^*=80 (side view) (c) t^*=80 (top view) (d) t^*=85 (e) t^*=190 and (f) t^*=195 and (g) von Mises equivalent plastic strain plot of the microstructure in (d). Martensite variants -1,2 and 3 are shown in red, blue and green, respectively. Austenite on the $(111)^{\gamma}$ plane is shown in white. Arrows point towards the areas where reversion occurs.

Sachs (K-S) orientation relationship (OR), can be grouped into three basic variants known as Bain variants [32–34]. In order to simulate 24 different martensite variants, the model needs to consider 24 phase-field variables, which increases the computational complexity of the model. Therefore in the present work three phase-field variables (η_1, η_2, η_3) that correspond to the three Bain variants, which form the basis for the K-S OR, are considered [24].

The Gibbs energy of a system undergoing athermal martensitic transformation can be expressed as:

$$G = \int_V (G_v^{chem} + G_v^{grad} + G_v^{el})dV \tag{2}$$

where G_v^{chem} corresponds to the chemical part of the Gibbs energy density, $G^{grad}{}_v$ is the gradient energy term, $G^{el}{}_v$ is the elastic strain energy density.

G_v^{chem} is expressed as a Landau-type polynomial [20,21]:

$$G_v^{chem}(\eta_1, \eta_2, \eta_3) = \frac{1}{V_m}\left[\frac{1}{2}A(\eta_1^2 + \eta_2^2 + \eta_3^2) \quad -\frac{1}{3}B(\eta_1^3 + \eta_2^3 + \eta_3^3) + \frac{1}{4}C(\eta_1^2 + \eta_2^2 + \eta_3^2)^2\right] \tag{3}$$

where V_m is the molar volume and the coefficients A, B, C are expressed in terms of Gibbs energy barrier and the driving force [20].

G_v^{grad} is expressed as [20,21]:

$$G_v^{grad} = \frac{1}{2}\sum_{p=1}^{p=3}\beta_{ij}(p)\frac{\partial\eta_p}{\partial r_i}\frac{\partial\eta_p}{\partial r_j} \tag{4}$$

where $\mathbf{r}(\mathbf{x}, \mathbf{y}, \mathbf{z})$ is the position vector expressed in Cartesian coordinates. β_{ij} is the gradient coefficient matrix expressed in terms of the interfacial energy, molar volume and the Gibbs energy barrier.

G_v^{el} can be expressed as [20,23]:

$$G_v^{el} = \int_{\epsilon_{ij}^0(\mathbf{r})}^{\epsilon_{ij}(\mathbf{r})} c_{ijkl}(\epsilon_{kl}(\mathbf{r}) - \epsilon_{kl}^0(\mathbf{r}) - \epsilon_{kl}^{pl}(\mathbf{r}))d\epsilon_{ij}(\mathbf{r}) \tag{5}$$

where c_{ijkl} is the tensor of elastic constants, $\epsilon_{ij}(\mathbf{r})$ is the total strain, $\epsilon_{kl}^{pl}(\mathbf{r})$ is the plastic strain and $\epsilon_{ij}^0(\mathbf{r})$ is the stress-free transformation strain expressed in terms of η_q and Bain strains (ϵ_{ij}^{00}).

The material undergoes plastic deformation when the internal stress exceeds the yield limit. The evolution of plastic strain $\epsilon_{ij}^{pl}(\mathbf{r})$ is governed by [20,23]:

$$\frac{\partial\epsilon_{ij}^{pl}(\mathbf{r})}{\partial t} = -k_{ijkl}\frac{\delta G_v^{shear}}{\delta\epsilon_{kl}^{pl}(\mathbf{r})} \tag{6}$$

where G_v^{shear} is the shear energy density and k_{ijkl} is the plastic kinetic coefficient.

Linear isotropic strain hardening is considered by using the following expression [35]:

$$\sigma_y = \sigma_y^0 + H\epsilon^{pl}(\mathbf{r}) \tag{7}$$

where σ_y is yield stress of the material that depends on plastic strain, σ_y^0 is initial yield stress, H is hardening modulus and $\epsilon^{pl}(\mathbf{r})$ is von Mises equivalent plastic strain.

Finally the total strain is calculated by solving the mechanical equilibrium equation:

$$c_{ijkl}\left(\frac{\partial\epsilon_{kl}}{\partial r_j} - \sum_{p=1}^{p=v}\epsilon_{kl}^{00}(p)\frac{\partial\eta_p(\mathbf{r})}{\partial r_j} - \frac{\partial\epsilon_{kl}^{pl}(\mathbf{r})}{\partial r_j}\right) = 0 \tag{8}$$

The following input simulation data corresponding to stainless steels with a composition of Fe-17 wt%Cr-7 wt%Ni are acquired from different sources, such as CALPHAD, ab initio calculations and experiments [25,29]: A=1188 J/mol, B=3564 J/mol, C=2376 J/mol, β=0.1061×10^{-10} J/m; Bain strains are $\epsilon_1 = 0.1316$, $\epsilon_3 = -0.1998$; elastic constants of austenite are C_{11} = 209 GPa, C_{12} = 133 GPa and C_{44} = 121 GPa; elastic constants of martensite are C_{11} = 248 GPa, C_{12} = 110 GPa and C_{44} = 120 GPa; σ_y^0 (austenite)=500 MPa, σ_y^0 (martensite)=800 MPa, H=738 MPa, k=0.2GPa^{-1}s^{-1}, driving force=−3600 and +150 J/mol at T=263 K and 975 K, respectively.

A single crystal of austenite of 1 μm grain size is subjected to several thermal cycles with temperature varying between 263 K and 975 K as shown in Fig. 1a. The same process is repeated under two different conditions, viz. (a) with and (b) without strain hardening in order to study its effect on the transformation. A pre-existing martensite embryo is considered in the center of the grain, in order to maintain the symmetry in the cubic grain. Dirichlet (clamped) boundary conditions are considered. Simulations are performed on a 50×50×50 mesh by using FemLego software [36]. Due to the lack of available experimental data on the kinetics of lath martensite, L_{pq} in Eq. (1) is considered to be unity and the microstructure evolution is discussed in terms of dimensionless time, t*.

3. Results and discussion

Fig. 1b (side view) and 1c-f (top view) shows the microstructures obtained during different stages of thermal cycling shown in Fig. 1a. Martensite laths (variants), plotted in red, blue and green, are formed during quenching (Fig. 1b). The regions where martensite has formed during quenching are marked by a boundary on the $(111)^{\gamma}$ plane (Fig. 1c and e) and these boundaries are superimposed on the microstructures obtained after the corresponding thermal cycles (Fig. 1d and f), i.e. microstructure boundary in Fig. 1c is superimposed on Fig. 1d and the boundary in Fig. 1e is superimposed on Fig. 1f. The regions in white that lie inside the boundary in Fig. 1d and f correspond to reversed austenite, whereas the regions in white that lie outside the boundary correspond to retained austenite. Fig. 1d shows that martensite units revert to austenite (circles, rectangles and arrows) during heating. Some martensite units (compare Fig. 1c and d) completely revert (rectangles), whereas some partially revert to austenite (circles). Reversion initiates at lath boundaries, where a low nucleation energy is sufficient to overcome the transformation barrier (Fig. 1d and f) [29]. Reversion proceeds by interface migration, which is in good agreement with Durlu's experimental study on Fe-Ni-C alloy [13]. Martensite units that are surrounded by retained austenite (arrows in Fig. 1d and f) offer less resistance to reversion and hence revert more compared to the martensite units that are surrounded by other martensite units (big variant in red at the center). Reversion of martensite is prominent during early stages of thermal cycling (compare Fig. 1c and d), whereas less volume fraction of martensite reverts to austenite during the later stages of thermal cycling (compare Fig. 1e and f). Fig. 1g shows the von Mises equivalent plastic strain plot corresponding to the microstructure shown in Fig. 1d. Although some regions in the microstructure have reversed to austenite (Fig. 1d), plastic strains created during martensite formation are retained in the reversed austenite [29]. This plot also shows that a martensitic lath-like structure is inherited by the reversed austenite.

Fig. 2 shows variations in volume fraction of martensite with dimensionless time t* during pure quenching and thermal cycling. In the case of thermal cycling, during the heating stage of each thermal cycle, the martensite volume fraction decreases due to reversion of martensite to austenite. The volume fraction of martensite that reverts to austenite decreases with increasing number of thermal cycles, as also observed in microstructures (Fig. 1), and suggests an increased stability of martensite. It also suggests that the surrounding retained austenite resists the reversion of martensite, implying an increased strength and stability of austenite. The differences in martensite volume fraction obtained during pure quenching and thermal cycling also suggest that thermal cycling leads to strengthening of austenite and hence less volume fraction of martensite is formed.

Fig. 3 shows variations of the mean von Mises equivalent stress, strain and plastic strain in austenite and martensite, with the number of thermal cycles. The mean von Mises equivalent stress (Fig. 3a) in

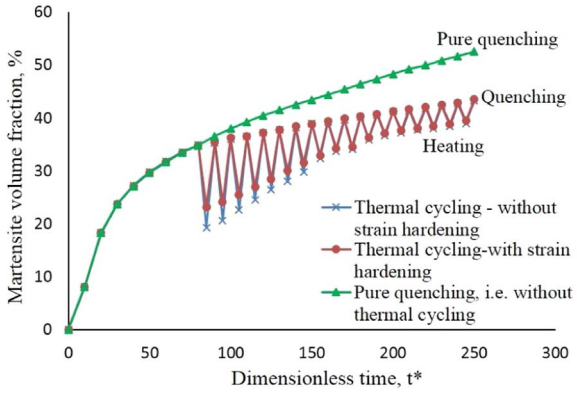

Fig. 2. Variation in martensite volume fraction.

martensite decreases with increasing number of thermal cycles, due to the relaxation provided by reversion during heating. The internal stresses in martensite can add to the driving force for formation of austenite and can lead to reversion of martensite [29]. However, in the present case the equivalent stress in martensite decreases, which implies less driving force for formation of austenite. Hence martensite becomes more stable with increasing number of thermal cycles (Fig. 2). The von Mises equivalent stress in austenite does not show significant variations, although it slightly increases compared to the as-quenched case (cycle-0).

The mean von Mises equivalent strain (Fig. 3b) in martensite decreases with increasing number of thermal cycles, due to stress relaxation as shown in Fig. 3a. However, von Mises equivalent strain in austenite increases significantly. The increased strain in austenite increases the strain energy, which opposes the chemical energy (thermodynamic driving force for martensite formation) and thus martensite formation becomes more difficult. This requires an increased driving force, which implies a decrease in M_s temperature. This is in good agreement with the experimental study of Hidalgo and Santofimia, who observed that M_s temperature of Fe-C-Si steel decreases with increasing number of thermal cycles due to strengthening of austenite [10]. Lee has also observed that the M_s temperature of an Fe-Mn alloy decreases with increasing number of thermal cycles [37].

In the experimental work presented in Ref. [10], the strengthening of austenite is mainly attributed to grain refinement. In the present simulations the prior austenite grain size is kept constant during thermal cycling. Although some regions in the prior austenite grain transform to martensite and back to reversed austenite (Fig. 1d) and thereby give rise to finer austenite grains (grain refinement), the strengthening of austenite due to grain refinement (Hall-Petch effect) is not considered in this work. Hence grain refinement cannot be the reason for the strengthening of austenite. Alternatively, plasticity and strain hardening contribute to the strengthening of austenite. The mean von Mises equivalent plastic strains (dislocation density) in both austenite and martensite increase with increasing number of thermal cycles (Fig. 3c). Hidalgo and Santofimia observed that dislocation density increases with decreasing grain size due to thermal cycling of an Fe-C-Si steel [10]. Several other experimental studies also showed that dislocation density increases with thermal cycling of steels [13,14,37]. Lee [37] has reported that the increase in dislocation density increases the shear stress, which requires larger driving force for martensite formation and thereby decreases the M_s temperature.

The increase in plastic strains, i.e. dislocation density, leads to strain hardening and thereby contributes to the strengthening of austenite. The effect of strain hardening on strength of austenite can be seen in Fig. 2. In the absence of strain hardening, the 'weaker' austenite facilitates reversion of martensite more easily compared to the 'stronger' strain hardened austenite. In the absence of strain

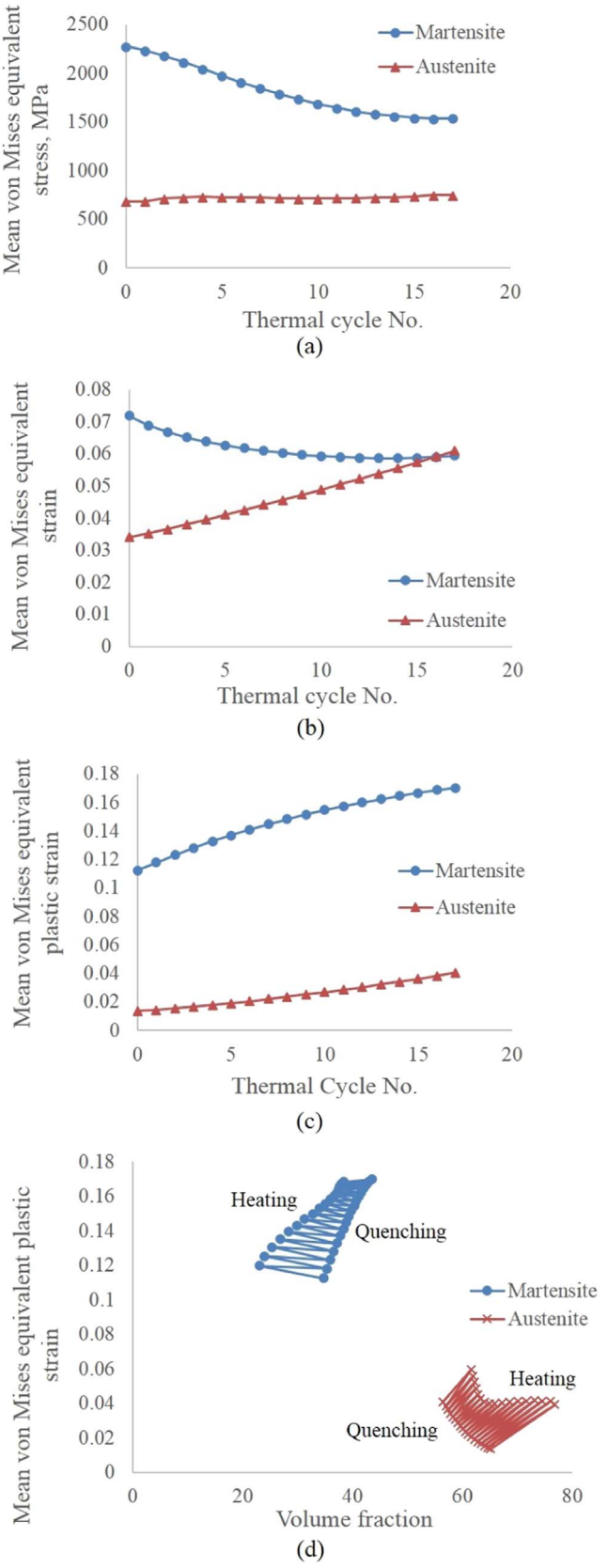

Fig. 3. Variation of mean von Mises equivalent (a) stress (b) strain (c) plastic strain with thermal cycles (d) variation of mean von Mises equivalent plastic strain with volume fraction.

hardening, several thermal cycles are needed for accumulation of plastic strains and for the material to be strong enough to resist reversion of martensite. In the presence of strain hardening, the strain hardening of the material provides an extra resistance to reversion of martensite already from the initial stages of thermal cycling. Thus during the initial stages of thermal cycling, there is a visible difference between the martensite volume fractions obtained in the two cases (Fig. 2). However, during the later stages of thermal cycling, the material in both cases is strong enough to resist reversion and hence the difference in volume fractions obtained in the two cases decreases.

During reversion in a given thermal cycle, the equivalent plastic strain in austenite increases more compared to that in martensite (Fig. 3d). In the 301-type steel studied in the present work, reversion occurs through a shear mechanism and therefore dislocations are inherited from martensite to reversed austenite and hence the observed difference in the equivalent plastic strains [2,5,29]. Moreover, since the highly dislocated martensite is less effective in accommodating plastic strains during reversion, austenite deforms more compared to martensite, which is in agreement with Ref. [10].

4. Conclusions

The phase-field simulations show that martensite becomes more stable with increasing number of thermal cycles, due to decreasing stresses in martensite and due to strengthening of austenite. Austenite strengthening is due to increase in plastic strain, i.e. dislocation density, which leads to strain hardening of the material. The strain in austenite increases with increasing number of thermal cycles and increases the energy barrier for martensitic transformation, implying a decreased M_s temperature. The results are in good agreement with experimental observations, such as increase in dislocation density and strengthening of austenite with increasing number of thermal cycles [10,37]. Lee [37] has reported that the increase in dislocation density increases the shear stress and thereby decreases the M_s temperature.

In reality, austenite grains (typically around 10 – 50 μ) contain lath martensite that forms in blocks and packets, which also act as barriers for dislocation motion. It is not possible to observe this hierarchic pattern formation in the simulated microstructures, due to the small grain size of 1 μ. Nevertheless, an encouraging correlation between the trends in the present simulations and experimental works is obtained, which highlights the effect of thermal cycling on strengthening of stainless steels. In the future, it would be interesting to model the effect of thermal cycling on martensitic transformation in polycrystalline steels.

Acknowledgements

This work made use of the facilities of N8 HPC Centre of Excellence, provided and funded by the N8 consortium and EPSRC (Grant No. EP/K000225/1). The Centre is co-ordinated by the Universities of Leeds and Manchester. DHRTC at DTU is acknowledged for financial support.

References

[1] R.D.K. Misra, Z. Zhang, P.K.C. Venkatasurya, M.C. Somani, L.P. Karjalainen, Martensite shear phase reversion-induced nanograined/ultrafine-grained Fe-16Cr-10Ni alloy: the effect of interstitial alloying elements and degree of austenite stability on phase reversion, Mater. Sci. Eng. A 527 (2010) 7779–7792.
[2] F. Forouzan, A. Najafizadeh, A. Kermanpur, A. Hedayati, R. Surkialiabad, Production of nano/submicron grained AISI 304L stainless steel through the martensite reversion process, Mater. Sci. Eng. A 527 (2010) 7334–7339.
[3] R.D.K. Misra, S. Nayak, P.K.C. Venkatasurya, V. Ramuni, M.C. Somani, L.P. Karjalainen, Nanograined/ultrafine-grained structure and tensile deformation behavior of shear phase reversion-induced 301 austenitic stainless steel, Met. Mater. Trans. A 41 (2010) 2162–2174.
[4] K. Tomimura, S. Takaki, Y. Tokunaga, Reversion mechanism from deformation induced martensite to austenite in metastable austenitic stainless-steels, ISIJ Int. 31 (1991) 1431–1437.
[5] H. Shirazi, G. Miyamoto, S.H. Nedjad, H.G. Nanesa, M.N. Ahmadabadi, T. Furuhara, Microstructural evaluation of austenite reversion during intercritical annealing of Fe-Ni-Mn martensitic steel, J. Alloy. Compd. 577 (2013) S572–S577.
[6] A.D. Schino, M. Barteri, J.M. Kenny, Development of ultra fine grain structure by martensitic reversion in stainless steel, J. Mat. Sci. Lett. 21 (2002) 751–753.
[7] D. Raabe, S. Sandlöbes, J. Millan, D. Ponge, H. Assadi, M. Herbig, P.P. Choi, Segregation engineering enables nanoscale martensite to austenite phase transformation at grain boundaries: a pathway to ductile martensite, Acta Mater. 61 (2013) 6132–6152.
[8] S.M.C. Van Bohemen, J. Sietsma, Kinetics of martensite formation in plain carbon steels: critical assessment of possible influence of austenite grain boundaries and autocatalysis, Mater. Sci. Tech. 30 (2014) 1024–1033.
[9] W. Hui, Microstructure refining and strengthening of martensitic steel, in: Yuqing Weng (Ed.), Ultra-Fine Grained Steels, Springer Berlin Heidelberg, 2009, pp. 300–349.
[10] J. Hidalgo, M.J. Santofimia, Effect of prior austenite grain size refinement by thermal cycling on the microstructural features of as-quenched lath martensite, Met. Mater. Trans. A (2016). http://dx.doi.org/10.1007/s11661-016-3525-4.
[11] S.C. Kennett, G. Krauss, K.O. Findley, Prior austenite grain size and tempering effects on the dislocation density of low-C Nb-Ti microalloyed lath martensite, Scr. Mater. 107 (2015) 123–126.
[12] M. Villa, T.L. Christiansen, M.F. Hansen, M.A.J. Somers, Investigation of martensite formation in Fe based alloys during heating from boiling nitrogen temperature, J. Heat. Treat. Mater. 71 (2016) 12–19.
[13] T.N. Durlu, The effect of thermal cycling on the strength of austenitic Fe-Ni-C single crystals, Scr. Met. 15 (1981) 383–386.
[14] A. Alaei, H. Jafarian, A.R. Eivani, Observation austenite memory and significant enhancement of tensile properties during cyclic reverse martensite transformation in a Fe-Ni-C TRIP steel, Mater. Sci. Eng. A 676 (2016) 342–350.
[15] J.R.C. Guimaraes, P.R. Rios, The mechanical-induced martensite transformation in Fe-Ni-C alloys, Acta Mater. 84 (2015) 436–442.
[16] M.X. Huang, O. Bouaziz, D. Barbier, S. Allain, Modelling the effect of carbon on deformation behavior of twinning induced plasticity steels, J. Mater. Sci. 46 (2011) 7410–7414.
[17] H. Hallberg, P. Håkansson, M. Ristinmaa, A constitutive model for the formation of martensite in austenitic steels under large strain plasticity, Int. J. Plast. 23 (2007) 1213–1239.
[18] L.Q. Chen, Phase-field models for microstructure evolution, Annu. Rev. Mater. Res. 32 (2002) 113–140.
[19] S. Minamoto, S. Nomoto, A. Hamaya, T. Horiuchi, S. Miura, Microstructure simulation for solidification of magnesium-zinc-yttrium alloy by multiphase-field method coupled with CALPHAD database, ISIJ Int. 50 (2010) 1914–1919.
[20] H.K. Yeddu, A. Malik, J. Ågren, G. Amberg, A. Borgenstam, Three-dimensional phase-field modeling of martensitic microstructure evolution in steels, Acta Mater. 60 (2012) 1538–1547.
[21] A. Artemev, Y. Jin, A.G. Khachaturyan, Three-dimensional phase field model of proper martensitic transformation, Acta Mater. 49 (2001) 1165–1177.
[22] H.K. Yeddu, A. Borgenstam, J. Ågren, Effect of martensite embryo potency on the martensitic transformations in steels - A 3D phase-field study, J. Alloy. Compd. 577S (2013) S141–S146.
[23] A. Yamanaka, T. Takaki, Y. Tomita, Elastoplastic phasefield simulation of self- and plastic accommodations in cubic tetragonal martensitic transformation, Mater. Sci. Eng. A 491 (2008) 378–384.
[24] H.K. Yeddu, A. Borgenstam, J. Ågren, Stress-assisted martensitic transformations in steels: a 3-D phase-field study, Acta Mater. 61 (2013) 2595–2606.
[25] H.K. Yeddu, V.I. Razumovskiy, A. Borgenstam, P.A. Korzhavyi, A.V. Ruban, J. Ågren, Multi-length scale modeling of martensitic transformations in stainless steels, Acta Mater. 60 (2012) 6508–6517.
[26] K. Ankit, T. Mittnacht, R. Mukherjee, B. Nestler, Evolution of mixed cementite morphologies during non-cooperative eutectoid transformation in Fe-C steels, Comp. Mat. Sci. 108 (2015) 342–347.
[27] H.K. Yeddu, H. Zong, T. Lookman, Alpha - omega and omega - alpha phase transformations in zirconium under hydrostatic pressure: a 3D mesoscale study, Acta Mater. 102 (2016) 97–107.
[28] H.K. Yeddu, T. Lookman, Phase-field modeling of the beta to omega phase transformation in Zr-Nb alloys, Mater. Sci. Eng. A 634 (2015) 46–54.
[29] H.K. Yeddu, T. Lookman, A. Saxena, Reverse phase transformation of martensite to austenite in stainless steels: a 3D phase-field study, J. Mater. Sci. 49 (2014) 3642–3651.
[30] P. Song, Y. Ji, L. Chen, W. Liu, C. Zhang, L.Q. Chen, Z. Yang, Phase-field simulation of austenite growth behavior: Insights into the austenite memory phenomenon, Comp. Mat. Sci. 117 (2016) 139–150.
[31] H.K. Yeddu, T. Lookman, A. Saxena, The simultaneous occurrence of martensitic transformation and reversion of martensite, Mater. Sci. Eng. A 594 (2014) 48–51.
[32] Z. Guo, C.S. Lee, J.W. Morris Jr., On coherent transformations in steel, Acta Mater. 52 (2004) 5511–5518.
[33] P.P. Suikkanen, C. Cayron, A.J. DeArdo, L.P. Karjalainen, Crystallographic analysis of martensite in 0.2C-2.0Mn-1.5Si-0.6Cr steel using EBSD, J. Mater. Sci. Tech. 27 (2011) 920–930.
[34] H.K. Yeddu, (Ph.D. thesis), Martensitic transformations in steels - A 3D phase-field study, KTH Royal Institute of Technology, Sweden, 2012.
[35] E.A. De souza Neto, D. Peric, D.R.J. Owen, Computational Methods for Plasticity - Theory and applications, John Wiley and Sons Ltd., West Sussex (UK), 2008.
[36] G. Amberg, R. Tönhardt, C. Winkler, Finite element simulations using symbolic computing, Math. Comp. Sim 49 (1999) 257–274.
[37] Y.K. Lee, Relationship between austenite dislocation density introduced during thermal cycling and Ms temperature in an Fe-17 Wt Pct Mn alloy, Metall. Trans. A 33 (2002) 1913–1917.